

Numerical simulations of nonlinear MHD body and surface waves in magnetic slabs

P. Huang¹, Z.E. Musielak^{1,2,3}, and P. Ulmschneider³

¹ Center for Space Plasma, Aeronomy and Astrophysics Research, University of Alabama, Huntsville, AL 35899, USA

² Physics Department, University of Texas at Arlington, Arlington, TX 76019, USA

³ Institut für Theoretische Astrophysik der Universität Heidelberg, Tiergartenstrasse 15, D-69121 Heidelberg, Germany

Received 15 July 1998 / Accepted 21 October 1998

Abstract. The behavior of MHD waves propagating in magnetically structured plasmas has been extensively investigated in the literature. In most of these studies, the wave treatment was restricted to the linear regime. This paper presents the results of time-dependent and nonlinear numerical simulations of MHD body and surface waves propagating along magnetic slabs. Both longitudinal and transverse waves are computed, and the wave behavior in the linear and nonlinear regime is compared. Two physical processes are investigated in detail. The first is the energy leakage from the magnetic slab to the field-free external medium. It is found that the energy leakage is 62% for transverse slab waves, which means that the efficiency of energy transfer along the slab by these waves is significantly reduced. The second process is the excitation of MHD waves in two adjacent magnetic slabs by large amplitude acoustic waves from the external medium. The slabs have physical parameters typical for photospheric magnetic flux tubes. It is shown that only 1–3% of the energy carried by these acoustic waves is transferred to the slabs, and that the efficiency of this process strongly depends on the location of the slabs relative to the source of acoustic waves and on the amplitude of these waves. Both physical processes are important for the problem of heating of magnetically structured regions in the solar and stellar atmospheres.

Key words: waves – Sun: corona – Sun: chromosphere – methods: numerical – Sun: magnetic fields – MHD

1. Introduction

Magnetohydrodynamic (MHD) surface and body waves are known to be important in laboratory plasmas, in magnetospheric physics and in astrophysics (Lanzerotti et al. 1973; Chen & Hasegawa 1974; Lanzerotti & Southwood 1979; Takahashi & McPherron 1984; Bertin & Coppi 1985; Musielak & Suess 1988; Roberts 1991; Goedbloed & Halberstadt 1994; Goossens 1994; Narain & Ulmschneider 1996; Poedts & Goedbloed 1997; Poedts et al. 1997). The observations of solar magnetic field

structures, such as magnetic flux tubes, sunspots, coronal loops and coronal holes, indicate that discontinuities exist on the Sun (Stenflo 1978; Zwaan 1989; Solanki 1993). These discontinuities can support MHD surface waves; the role of these waves in chromospheric and coronal heating has been extensively explored in the literature. It has been suggested that propagating MHD body and surface waves may supply large amounts of energy from the subphotospheric layers (generated there by turbulent convection) to the upper atmospheric layers. This wave energy is thought to be dissipated in the coronal plasma by mode-coupling, resonance as well as turbulent heating in the case of body waves and through resonant absorption and phase-mixing in the case of surface waves (see Narain & Ulmschneider 1996, and references therein).

Previous studies have been primarily concerned with three different models of structured magnetic field configurations, namely, magnetic interfaces, magnetic slabs and magnetic flux tubes. In this paper, the propagation of MHD waves along magnetic interfaces and slabs is considered, however, see Spruit (1981), Spruit & Roberts (1983), Herbold et al. (1985), Ulmschneider et al. (1991), and Ziegler & Ulmschneider (1997a, b) for discussions of the propagation of MHD waves along magnetic flux tubes. For linear MHD surface waves on a single magnetic interface, the resulting dispersion relations have been derived and studied by Roberts & Webb (1978), Wentzel (1979) and Roberts (1981a). The studies show that on such magnetic structures, body waves can either be longitudinal or transverse depending upon the type of perturbation imposed, and that surface waves can be either slow or fast depending on the relative magnitude of the temperatures on both sides of the interface. Time-dependent analytical solutions of the initial value problem for linear MHD surface waves on a single magnetic interface have been found by Lee & Roberts (1986) for the case of an incompressible background medium.

The propagation of MHD surface and body waves in magnetic slabs is much more complicated than that on a single magnetic interface due to the richness of modes that can exist in such magnetic field structures (Roberts 1981b), and due to the fact that these slabs can effectively interact with the external medium. The latter means that a two-dimensional treatment is required and, as a result, the mathematical description may be-

Send offprint requests to: P. Ulmschneider

Correspondence to: ulm@ita.uni-heidelberg.de

come too complicated to obtain analytical solutions even for simple physical situations. Hence, in most cases a numerical approach will be necessary. Such an approach was developed by Wu et al. (1996) who investigated the propagation of linear MHD body and surface waves along magnetic slabs embedded in an unstratified medium by using a two-dimensional, time-dependent numerical model. Their approach did not allow, however, for large amplitude perturbations.

To understand the behavior of nonlinear MHD body and surface waves, it is necessary to incorporate both the nonlinearity and the magnetic field discontinuities in the numerical model. Such a model has been developed and is described in this paper (see Sect. 2; also Huang 1995, 1996). The model allows simulating both linear and nonlinear MHD body and surface waves in the presence of background magnetic field discontinuities, however, without gravity. The numerical model is implemented as two-dimensional and can incorporate either single or multiple magnetic interfaces such as a magnetic slab or multiple magnetic slabs with any type of magnetic field variation inside the slab. There are no gradients in the physical quantities other than the presence of discontinuities in the background magnetic field and in the gas pressure to satisfy the pressure balance across these discontinuities. The considered numerical model is based on ideal MHD, which means that there is no wave energy dissipation. The numerical procedure and two tests performed to verify it are described in Sect. 3. The numerical simulations with their physical interpretation of our three model cases are discussed in Sects. 4 to 6. The conclusions are summarized in Sect. 7.

2. Physical models and governing equations

Three different physical models of increasing complexity are considered in this paper, namely, a single magnetic interface, a single magnetic slab and two adjacent magnetic slabs. In the *single interface model*, the background medium is separated by an interface into two regions with different strengths of the magnetic field; in a special case, the field can be zero in one of these regions. To satisfy the pressure balance across the interface, the gas pressure must be higher in the region where the magnetic field is weaker. It is assumed that the interface is located along the y -axis of a cartesian (x, y) coordinate system. A more detailed description of this model is given in Sect. 4, where it is used to verify the developed numerical code.

In the *single slab model*, two magnetic interfaces are introduced in the background medium to form a magnetic slab. The interfaces are located symmetrically with respect to the y -axis, so that the slab extends along that axis. The slab thickness is a free parameter in this approach and the external medium is assumed to be field-free. More details are given in Sect. 5, where the model is used to investigate the behavior of nonlinear MHD surface and body waves.

Finally, in the *two adjacent magnetic slabs model*, four interfaces are introduced in the background medium to form two slabs that are located parallel to the y -axis. Both slabs have the same thickness and the same strength of the magnetic field. The

external medium is again assumed to be field-free. More physical details of this model are given in Sect. 6, where the excitation of magnetic slab waves by external acoustic waves is discussed.

A mathematical description of the considered physical models is given by the set of ideal and two-dimensional MHD equations. After neglecting gravity, the set can be written in its conservative and dimensionless form (see Huang 1995) as follows

$$\frac{\partial \rho}{\partial t} + \frac{\partial(\rho V_x)}{\partial x} + \frac{\partial(\rho V_y)}{\partial y} = 0, \quad (1)$$

$$\begin{aligned} \frac{\partial(\rho V_x)}{\partial t} + \frac{\partial(\rho V_x^2)}{\partial x} + \frac{\partial(\rho V_x V_y)}{\partial y} = & -\frac{\partial \left[p + \frac{1}{\gamma\beta} (B_x^2 + B_y^2) \right]}{\partial x} \\ & + \frac{2}{\gamma\beta} \left[\frac{\partial B_x B_y}{\partial y} + \frac{\partial B_x^2}{\partial x} \right], \end{aligned} \quad (2)$$

$$\begin{aligned} \frac{\partial(\rho V_y)}{\partial t} + \frac{\partial(\rho V_x V_y)}{\partial x} + \frac{\partial(\rho V_y^2)}{\partial y} = & -\frac{\partial \left[p + \frac{1}{\gamma\beta} (B_x^2 + B_y^2) \right]}{\partial y} \\ & + \frac{2}{\gamma\beta} \left[\frac{\partial B_x B_y}{\partial x} + \frac{\partial B_y^2}{\partial y} \right], \end{aligned} \quad (3)$$

$$\frac{\partial B_x}{\partial t} = \frac{\partial(V_x B_y - V_y B_x)}{\partial y}, \quad (4)$$

$$\frac{\partial B_y}{\partial t} = -\frac{\partial(V_x B_y - V_y B_x)}{\partial x}, \quad (5)$$

$$\frac{\partial(p\rho^{1-\gamma})}{\partial t} + \frac{\partial(p\rho^{1-\gamma}V_x)}{\partial x} + \frac{\partial(p\rho^{1-\gamma}V_y)}{\partial y} = 0. \quad (6)$$

In this set, all variables are dimensionless and defined as follows: $\rho = \rho^d/\rho_o$, $p = p^d/\rho_o V_{So}^2$, $\mathbf{V} = \mathbf{V}^d/V_{So}$, $\mathbf{B} = \mathbf{B}^d/B_o$, $\mathbf{r} = \mathbf{r}^d/V_{So}t_o$ and $t = t^d/t_o$, where the superscript ‘‘d’’ refers to a dimensional quantity, and ρ is the gas density, \mathbf{V} is the velocity, p is the gas pressure, \mathbf{B} is the magnetic field strength, t is the time and \mathbf{r} is the position vector. The quantities ρ_o , B_o and V_{So} represent the reference density, magnetic field strength and sound speed, respectively, and t_o is the time scale. In addition, V_x and V_y are the components of the velocity, B_x and B_y are the components of the magnetic field strength, γ is the ratio of specific heats, and β is the ratio of gas pressure to magnetic pressure: $\beta = 8\pi p/B^2$. Initially there are no waves or fluid motions in the systems. The velocity perturbations (see Sects. 5 and 6) are introduced in the models at $t = 0$. Then, the unknowns ρ , V_x , V_y , B_x , B_y and p are computed as a function of x , y and t . The numerical procedure adopted to solve the governing MHD equations is described in the following section.

3. Numerical procedure

The governing MHD equations described in the previous section are of the hyperbolic type and can be cast in the form

$$U_t + F_x + G_y = 0, \quad (7)$$

where U represents a conservation quantity, and F and G flux components in x and y directions, respectively. The explicit version of the well-known MacCormack scheme, which is second order accurate in both time and space (Hirsch 1990), is used to discretize the above equation. According to this method, the predictor step is calculated from

$$\bar{U}_{i,j} = U_{i,j}^n - \tau_x(F_{i+1,j}^n - F_{i,j}^n) - \tau_y(G_{i,j+1}^n - G_{i,j}^n), \quad (8)$$

and the corrector step is given by

$$\bar{\bar{U}}_{i,j} = U_{i,j}^n - \tau_x(\bar{F}_{i,j} - \bar{F}_{i-1,j}) - \tau_y(\bar{G}_{i,j} - \bar{G}_{i,j-1}). \quad (9)$$

The final step is given as

$$U_{i,j}^{n+1} = \frac{1}{2}(\bar{U}_{i,j} + \bar{\bar{U}}_{i,j}), \quad (10)$$

where $\bar{F}_{i,j} = F(\bar{U}_{i,j})$, $\bar{G}_{i,j} = G(\bar{U}_{i,j})$, $\bar{\bar{F}}_{i,j} = F(\bar{\bar{U}}_{i,j})$, $\bar{\bar{G}}_{i,j} = G(\bar{\bar{U}}_{i,j})$, subscripts i, j are grid indices, $\tau_x = \Delta t / \Delta x$, $\tau_y = \Delta t / \Delta y$, where Δt is the time step, and Δx and Δy are grid spacings in x and y directions, respectively. For simplicity, a uniform grid will be used in this work. The grid spacing is chosen such that the wave structure is adequately resolved and the numerical dissipation inherent in the scheme is minimized.

A numerical scheme can either be implicit or explicit. For implicit schemes, the time step does not have to be restricted by the CFL (Courant, Friedrichs, Lewy) condition (Hirsch 1990). Therefore, these schemes are valuable for problems where fast convergence to a steady state is desired. However, a special attention must be given to the numerical iteration process. The explicit scheme is straightforward in implementation, but its disadvantage is that the time step has to satisfy the CFL condition. The latter states that the grid spacing cannot exceed the distance covered by a disturbance, traveling with maximum characteristic speed within the numerical time step utilized in the simulations (Hirsch 1990). For wave problems, the advantage of the implicit scheme is also not obvious because the time step is limited by the wave structure. In general, at least 15 grid points within a wavelength are needed to resolve the wave structure; if the time steps used in the simulations are too large, then meaningless (unphysical) results can be obtained. Thus, in this paper, the explicit version of the MacCormack scheme is used. The time step Δt_e from the CFL condition is given by

$$\Delta t_e < \min(\Delta x, \Delta y) / V_m, \quad (11)$$

where $V_m = \max(V_S, V_A)$ is the maximum of all characteristic wave speeds. V_A is the Alfvén speed.

For problems which involve discontinuities in the physical variables, numerical viscosity is needed in the explicit MacCormack scheme to achieve numerical stability. Hence, a numerical diffusion term in the form of $\mu \nabla^2 \Phi$, Φ being the velocity or the magnetic field strength, will be added to the original set of governing equations; μ is called ‘‘artificial viscosity’’. The introduction of artificial viscosity gives rise to another time step Δt_d . To obtain numerical stability of the central discretization of the numerical diffusion term, the following criterion has to be satisfied for two-dimensional problems (Hirsch 1990):

$$\mu \frac{\Delta t_d}{\min(\Delta x^2, \Delta y^2)} \leq \frac{1}{4}. \quad (12)$$

The appropriate time step Δt then is the smaller one of the two time steps Δt_e and Δt_d :

$$\Delta t = \min(\Delta t_e, \Delta t_d). \quad (13)$$

Having described the numerical procedure, it is now required to specify boundary conditions for the finite computational domain used in these numerical simulations. For the wave propagation problem, open boundary conditions are desired. Different methods have been used to implement these boundary conditions (see Forbes & Priest 1987, and references therein). A commonly used method is known as the Sommerfeld radiation condition. Among the many versions of this method, the simple approach developed by Orlandi (1976) has been successfully applied to many wave problems. In this approach, the wave propagation speeds of the various physical quantities at the boundary points are calculated by using values of these quantities at the nearby interior grid points. There is no inward propagation of information from outside the computational domain. If the Sommerfeld radiation condition is given by

$$U_t + c_U U_x = 0 \quad (14)$$

where U represents an arbitrary physical quantity and c_U the wave propagation speed, then the Orlandi prescription (note that the original Orlandi paper contains printing errors) is to compute

$$c_U = -\frac{\Delta x}{\Delta t} \frac{U_{i-1}^n - U_{i-1}^{n-2}}{U_{i-1}^n + U_{i-1}^{n-2} - 2U_{i-2}^{n-1}} \quad (15)$$

as well as

$$U_i^{n+1} = \frac{1 - \frac{\Delta t}{\Delta x} c_U}{1 + \frac{\Delta t}{\Delta x} c_U} U_i^{n-1} + \frac{2 \frac{\Delta t}{\Delta x} c_U}{1 + \frac{\Delta t}{\Delta x} c_U} U_{i-1}^n \quad (16)$$

using a leap-frog finite difference scheme.

Another important issue in solving MHD equations is the numerical treatment of the solenoidal condition. It is well-known that an incorrect numerical treatment of the induction equation may lead to a non-solenoidal magnetic field that varies in time and introduces a non-physical force along the field lines. Several numerical treatments have been proposed (Brackbill & Barnes 1980; Marder 1987; Evans & Hawley 1988). In the latter paper, the authors utilized a numerical technique called CT (Constrained Transport) that allows transforming the induction equation in such a way that it always maintains vanishing divergence of the field components to within machine round-off error. The CT technique is also adopted in this paper.

Before presenting the results of our numerical simulations, it is necessary to describe the time-dependent perturbations that are introduced in the computational domain to generate the wave motions. In this paper, only sinusoidal velocity perturbations are considered: $V(x_p, y_p, t) = \text{perc} \sin(2\pi t)$, where V is a dimensionless quantity and can either be V_x / V_{S_o} or V_y / V_{S_o} and perc represents the ratio between the velocity amplitude, V_o , and the reference sound speed, V_{S_o} . In addition, x_p and y_p represent the location of the velocity perturbation in the computational domain and will be specified for each considered case.

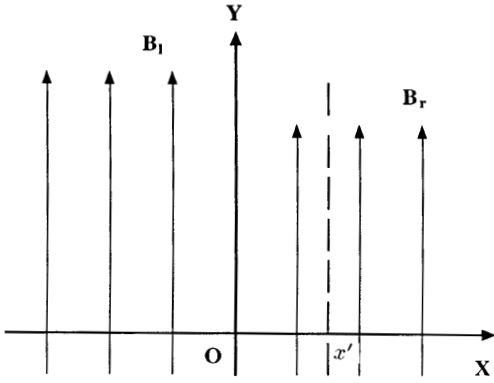


Fig. 1. Schematic description of single magnetic interface model used in the first test described in the main text.

4. Verification of numerical code

The results of two specific tests performed to verify the numerical code are presented in this paper (see Huang 1995, for more details and other tests). The first test involves the comparison of analytical and numerical results. In the second test, the results from two independent numerical codes are compared. In these tests two slightly different versions (see below) of the single magnetic interface model introduced in Sect. 2 are used.

The first test is to solve numerically an initial value problem for linear surface waves propagating along a single magnetic interface and compare the obtained results with the analytical solutions given by Lee & Roberts (1986). In their approach, a single magnetic interface is located in an incompressible and magnetized plasma. The interface separates the background medium into two regions of different magnetic fields, namely, B_l for $x < 0$ and B_r for $x > 0$ (see Fig. 1). Note that in the performed calculations both magnetic fields are normalized by B_o , which is taken to be either B_l or B_r whichever is stronger. To satisfy the pressure balance across the interface, the temperature on both sides of the interface is assumed to be different but the density is the same. Lee and Roberts introduced the following surface wave type perturbation at time $t = 0$ (see Fig. 1)

$$V_x(x, y, 0) = -Ae^{-|x-x'|} \sin(ky), \quad (17)$$

$$V_y(x, y, 0) = A(x-x')|x-x'|^{-1} e^{-|x-x'|} \cos(ky), \quad (18)$$

where $k = \pi\sqrt{2\gamma\beta}$, $A = 0.5 \text{ perc}$, $\text{perc} = 0.001$ and x' is the location of the vorticity line (see Fig. 1), which is the only place in the computational domain where vorticity is initially non-zero.

To reproduce these analytical results with our numerical code, it was necessary to run the code with $\beta = 100$ to account for incompressibility. We took $B_l = 1.0$ and $B_r = 0.5$. The comparison between analytical (upper panel) and numerical (lower panel) results is given in Figs. 2 and 3. As $V_A/V_S = \sqrt{2/(\gamma\beta)} = \text{rat}$, the number of points per wavelength of an Alfvén wave is given by $N_{AW} = \text{rat} N_W$, where N_W is the number of points per acoustic wavelength. We had to choose $N_W = 400$ to adequately resolve the Alfvén wave. With $N_x = 81$, $N_y = 120$ grid points in the computational

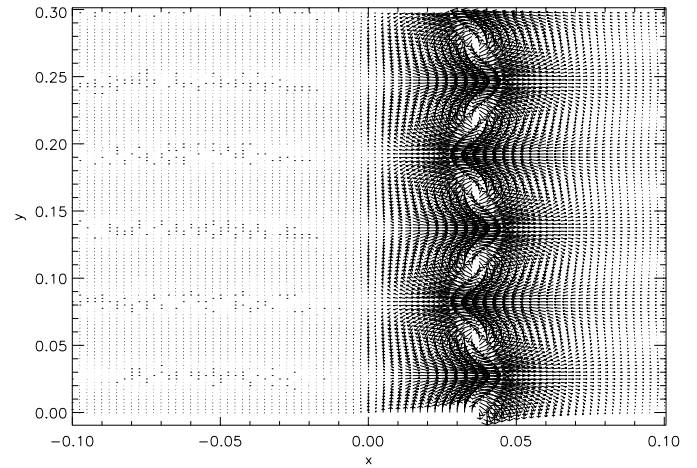
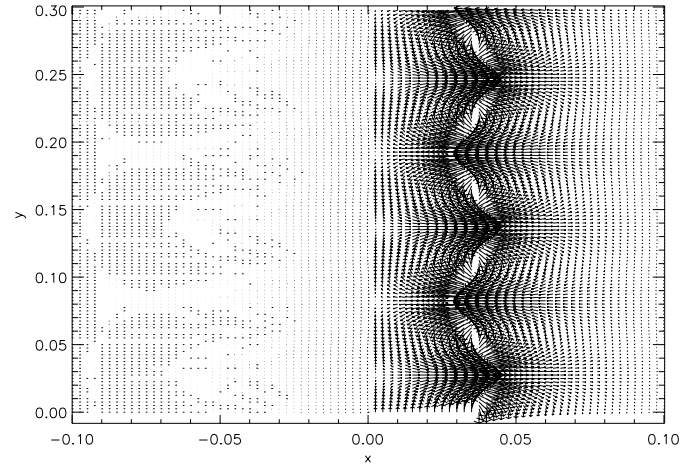


Fig. 2. The wave-induced velocity field calculated analytically (*upper panel*) and numerically (*lower panel*) at the location of the vorticity line ($x = x' = 0.375$) and in its vicinity. The presented results are snapshots taken at the dimensionless time $t = 1.0$.

domain we have used a grid spacing of $\Delta y = \Delta x = 1/N_W$. The vorticity line is at $x' = 0.036$. In Fig. 2, the velocity field at the location of the vorticity line and in its vicinity is shown. Fig. 3 shows the magnetic field perturbations at the interface and in its vicinity. It is clearly seen that the numerical results well reproduce the shape of the surface wave at the interface and the velocity and magnetic field patterns outside the interface. Some differences seen at the vorticity line can be explained by the effect of numerical viscosity and by the fact that the plasma β in numerical simulations is finite, whereas in the analytical treatment is infinite.

The second test is to numerically solve an initial value problem for MHD surface waves and compare the results with those obtained earlier by another numerical method. Here, the comparison is made with the numerical results obtained by Wu et al. (1996) who used a different numerical code. These authors considered a single magnetic interface that separates the background medium, which is compressible, into two domains: one with the magnetic field and one without it. They assumed that the temperature is constant on both sides of the interface, which

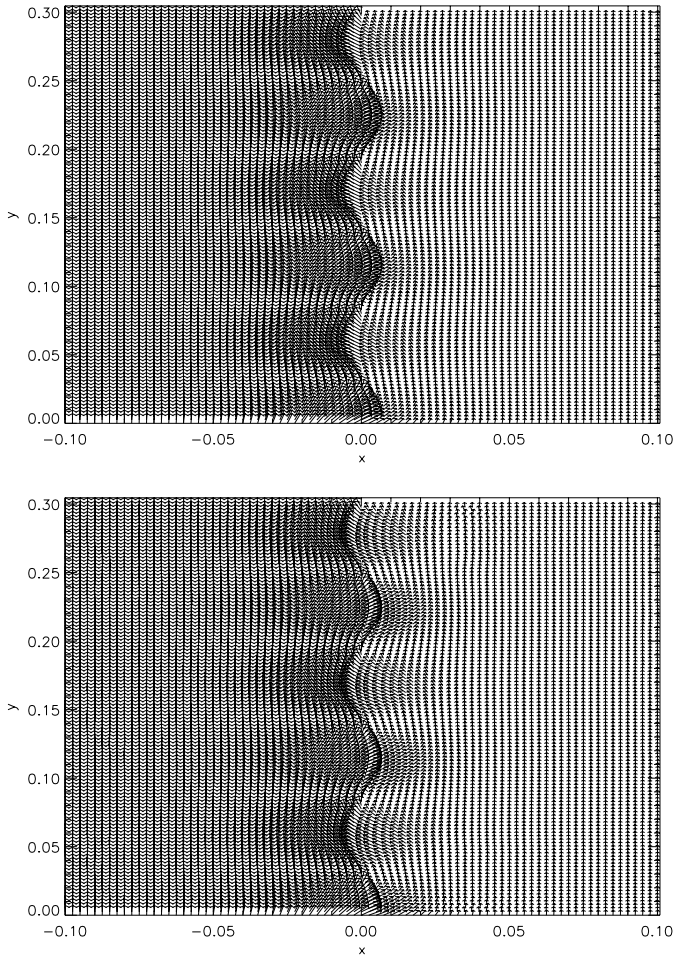


Fig. 3. The magnetic field perturbations calculated analytically (*top panel*) and numerically (*lower panel*) at the location of the interface ($x = 0.0$) and in its vicinity. The presented results are snapshots taken at the dimensionless time $t = 1.0$.

means that both domains must have different densities to satisfy the pressure balance across the interface. The numerical approach is limited to linear waves only. The comparison is made between the velocity field calculated by our code and that of Wu et al. (see Figs. 4 and 5). Here $\beta = 1.2$, $N_x = N_y = 66$, $N_W = 33$. The similarities in the overall pattern of the calculated velocity fields are clearly seen in these figures. The overall pattern of the computed magnetic field perturbations shows the same similarities and thus is not presented here. After testing the code against analytical and numerical solutions for linear MHD body and surface waves, we are now ready to investigate the behavior of nonlinear magnetic slab waves.

5. Nonlinear MHD slab waves

The single magnetic slab model already briefly introduced in Sect. 2 is used to investigate the behavior of MHD body and surface waves. In the model shown in Fig. 6, the magnetic slab with the physical parameters B_1 , P_1 , ρ_1 and T_1 is located at the center of the computational domain, with its axis aligned along the y -axis and with its thickness denoted by b . The external

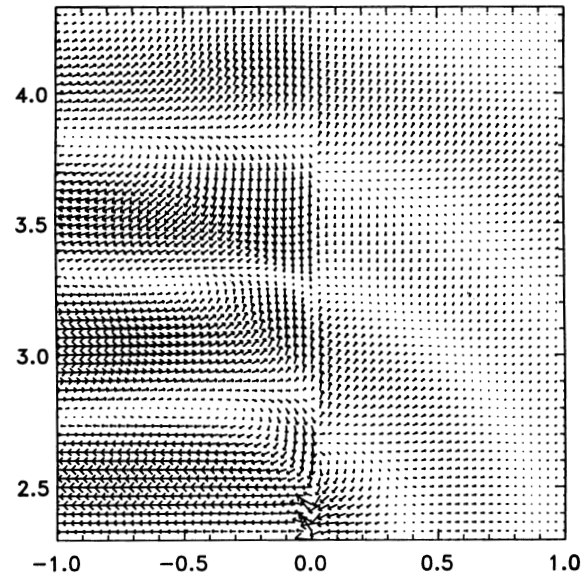


Fig. 4. Snapshot of the velocity field induced by a linear surface wave propagating along the magnetic interface. The presented results were obtained by using the code developed in this paper.

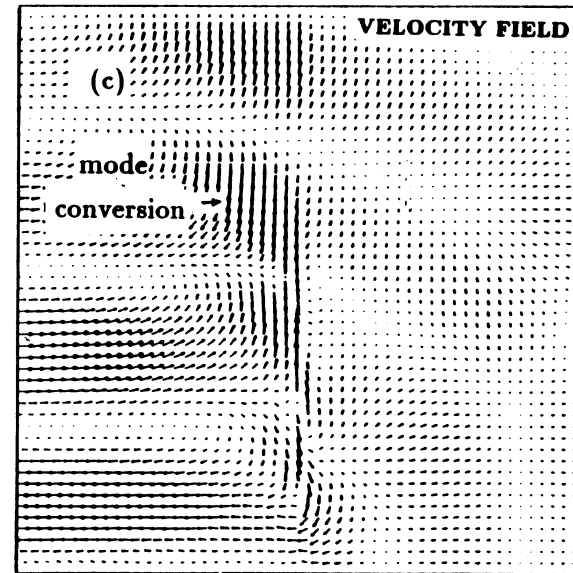


Fig. 5. The same as Fig. 4 but obtained by Wu et al. (1996).

medium is field-free, $B_{ext} = 0$, and has the same temperature as the slab, $T_{ext} = T_1$. The magnetic field inside the slab is uniform and the pressure balance in the x -direction is satisfied with the gas density ρ_1 lower than ρ_{ext} . The surface and body waves are generated by imposing longitudinal and transverse perturbations on the slab. In the performed numerical simulations, the slab thickness is assumed to be $b = 0.66$, which corresponds to two thirds of the acoustic wavelength, $\beta = 1$, and $N_W = 30$ grid points are chosen per acoustic wavelength to achieve a good numerical resolution of the generated waves. In addition, the CFL number (see the RHS of Eq. 11) is taken to be 0.4 and the numerical viscosity is chosen to be 0.01; the latter effectively minimizes numerical oscillations.

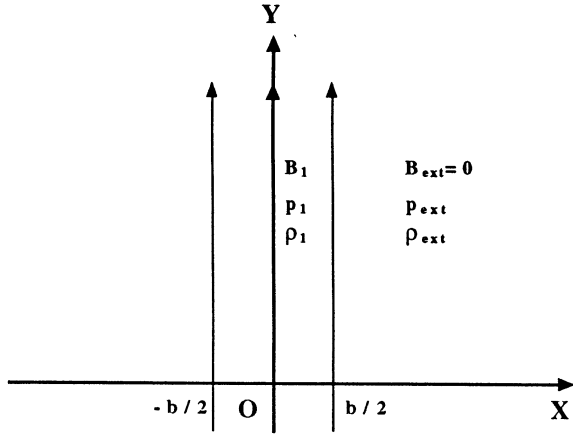


Fig. 6. Schematic description of single magnetic slab model used in numerical simulations described in the main text.

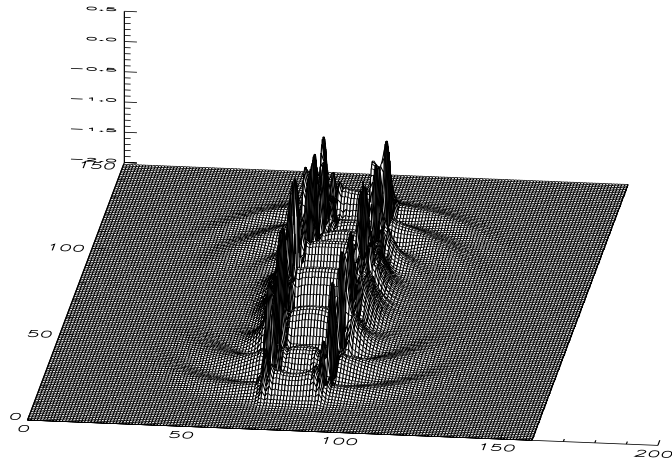


Fig. 7. Square of the velocity plotted on a logarithmic scale for a nonlinear wave generated by the longitudinal perturbation inside the magnetic slab with $perc = 0.2$ at the center of the computational domain.

5.1. Longitudinal perturbations

The following longitudinal velocity perturbations are imposed on the slab: $V_y(x_p, y_p, t) = perc \sin(2\pi t)$, at the center of the computational domain ($x_l \leq x_p \leq x_r, y_p = 2.5$), with $x_l = -b/2 = -.33, x_r = b/2 = .33$. Recall that t is the dimensionless time. The computational domain is given by $N_x = 161, N_y = 150$ points with grid distance $\Delta x = \Delta y = 1/N_W$. The perturbation extends over the entire width $b = x_r - x_l$ (of 20 points) of the magnetic slab region. As a result of these perturbations, V_x is initially zero. The velocity perturbation amplitude is assumed to be $perc=0.2$, that is 20% of the sound speed, which means that finite (nonlinear) amplitude waves are generated by the imposed motions.

The snapshots of the resulting velocity field and magnetic field perturbations at $t = 2.0$ are shown in Figs. 7 to 9. Fig. 7 shows the logarithm of the velocity square, that is, the quantity $Q = \log V^2 + 0.001$, where $V^2 = V_x^2 + V_y^2$. It is clearly seen in Fig. 7 that three types of waves are excited, namely, the internal body wave which is confined to the slab ($-0.33 < x < 0.33$),

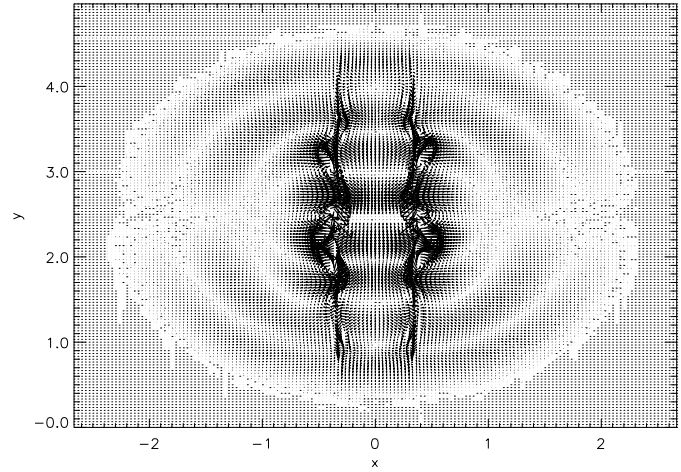


Fig. 8. The wave-induced velocity field generated by longitudinal perturbations with $perc = 0.2$ imposed on a single magnetic slab. Same as in Fig. 7, the snapshot is taken at the dimensionless time $t = 2.0$.

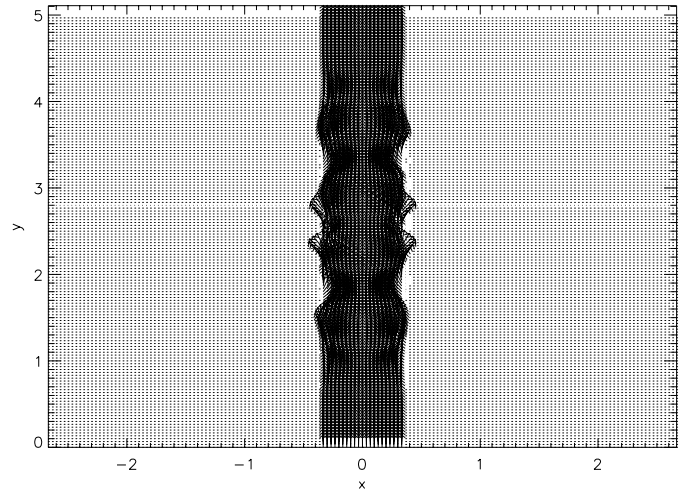


Fig. 9. The same as Figs. 7 and 8 but for the magnetic field perturbation.

the surface wave which propagates along the slab boundaries, and the external acoustic wave ($x < -0.33$ and $x > 0.33$) which is propagating isotropically in the external medium.

From a more detailed inspection of the velocity as seen in Fig. 8, one can see that the velocity inside the slab is essentially in the y -direction, which is the propagation direction of the internal body wave. This indicates that the internal body wave is longitudinal as expected from the imposed perturbation. The figure also shows some asymmetry in the resulting velocity field. This is caused by the fact that the longitudinal perturbations, which resemble a piston moving up and down, are imposed first in the upward direction leading thereby to the observed asymmetry in the velocity field. Note also that despite the fact that the initial perturbation is imposed only inside the slab there is significant wave energy leakage to the external medium; the latter is discussed separately in Sect. 6. The magnetic field perturbations displayed in Fig. 9 in the vicinity of the slab axis show the typical behavior of the sausage mode. Clearly, the longitudinal perturbation, which is in the direction of the magnetic field, does

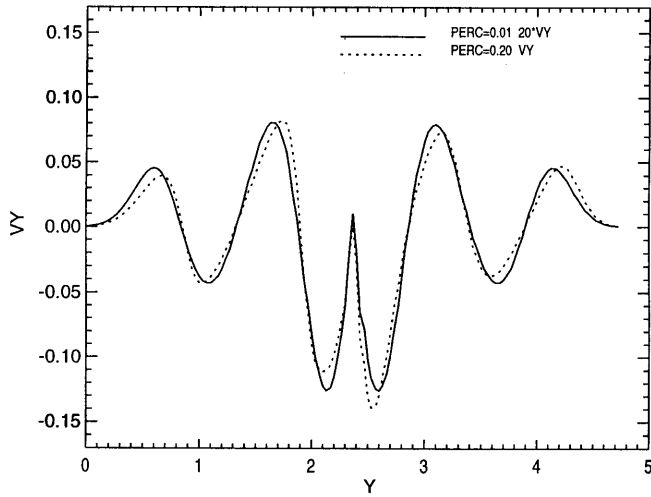


Fig. 10. Longitudinal velocity V_y is plotted versus y for linear and nonlinear waves generated by the longitudinal perturbation with $perc = 0.01$ and $perc = 0.2$, respectively. The results are shown for the dimensionless time $t = 2.0$ and at the location $x = 0$.

not disturb very much the magnetic field lines inside the slab but only at its boundaries, where the surface wave is generated.

Fig. 10 shows a comparison of the velocity V_y on the slab axis between the linear and nonlinear cases. The initial perturbation is imposed at $y = 2.5$. Longitudinal body waves are seen propagating along the slab axis in the upward ($y > 2.5$) and downward ($y < 2.5$) direction with respect to the location of the wave source. The steepening of the initially sinusoidal waves is evident in the case of the nonlinear perturbation ($perc = 0.2$) but it is not present for the linear case when $perc = 0.01$. The observed steepening is a consequence of the finite amplitude of the perturbations and will eventually result in the development of sawtooth shock waves. Note also that the decrease of the wave amplitude with distance from the wave source is caused by wave energy leakage to the external medium and the resulting excitation of external acoustic waves (see Sect. 6 for details).

5.2. Transverse perturbations

In this numerical simulation the physical parameters are the same as described above. The only difference is that the velocity perturbation is now transverse instead of longitudinal, which means that $V_y = 0$ and $V_x(x_p, y_p, t) = perc \sin(2\pi t)$, with $x_l \leq x_p \leq x_r$ and $y_p = 2.5$. The obtained results for the velocity field and magnetic field perturbations are shown in Figs. 11 to 13, respectively. As seen in Fig. 11, three types of waves are excited: the internal body wave, the surface wave on the slab boundaries and the external acoustic wave. The internal body wave is essentially transverse (see Fig. 12), which is easily understood considering the form of the imposed perturbation. Note that the surface wave is mainly longitudinal although the imposed perturbation is transverse. The latter and the “vortex structure” seen in this plot are caused by the transition of the fluid motion from the transverse body wave to the external

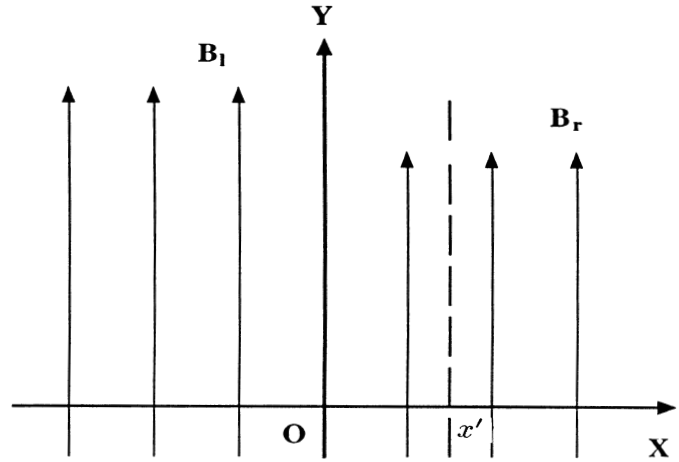


Fig. 11. Square of the velocity plotted on a logarithmic scale for a nonlinear wave generated by the transverse perturbation inside the magnetic slab with $perc = 0.2$ at the center of the computational domain.

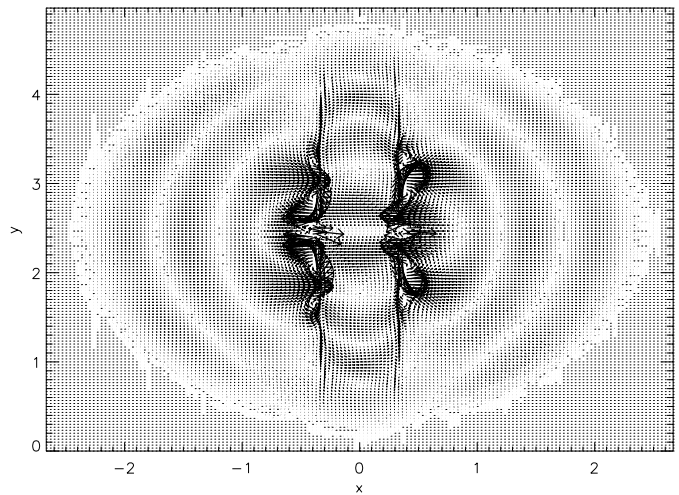


Fig. 12. The wave-induced velocity field generated by transverse perturbations with $perc = 0.2$ imposed on a single magnetic slab. Same as in Fig. 11, the snapshot is taken at the dimensionless time $t = 2.0$.

acoustic waves. There is also a prominent wave energy leakage to the external medium; see Sect. 6 for more details.

The observed asymmetry in the x -direction of the magnetic field can be explained by the fact that the very first perturbation is imposed to the right with respect to the slab axis. The swaying of the magnetic field lines which is a characteristic behavior of the kink mode is shown in Fig. 13. It is seen that the field lines act in unison, however, lines located closer to the slab boundaries lag behind. This is a typical behavior of the slow surface mode (see Roberts 1981b). Note that fast surface waves can only exist when the background medium is not isothermal, which is not the case considered here.

Fig. 14 shows the velocities V_x and V_y at the slab axis for the downward ($y > 2.5$) and upward ($y < 2.5$) propagating waves excited at $y = 2.5$. The amplitude of the transverse wave V_x decreases with distance from the wave source as a result of wave energy leakage to the external medium and due to the gen-

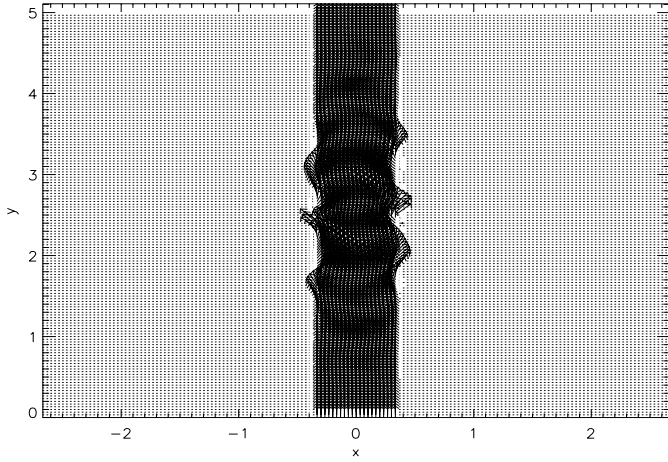


Fig. 13. The same as Figs. 11 and 12 but for the magnetic field perturbation.

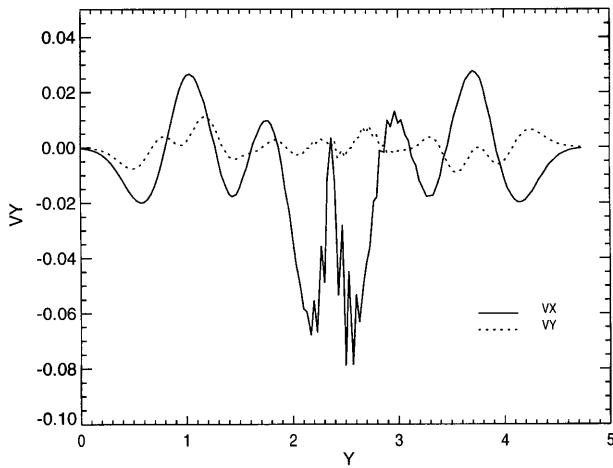


Fig. 14. Transverse V_x and longitudinal V_y velocities are plotted versus y for nonlinear waves generated by the transverse perturbation with $perc = 0.2$. The results are shown for the dimensionless time $t = 2.0$ and at the location $x = 0$.

eration of longitudinal waves V_y that propagate inside the slab. The process responsible for the excitation of these longitudinal waves is called nonlinear mode coupling and its efficiency has been investigated by Ulmschneider et al. (1991) in their one-dimensional numerical studies of the propagation of magnetic flux tube waves in the solar atmosphere. They suggested that the main reason for the appearance of longitudinal waves is the curvature force that results from the swaying of the magnetic field lines and is perpendicular to these lines. The consequence of this process is that the generated longitudinal waves take away part of the energy carried by the internal transverse body waves and, as a result, the latter are damped when they propagate. It must be noted that the longitudinal waves may form shocks and dissipate the wave energy leading thereby to the heating of the background plasma.

6. Applications to the Sun

It has long been known that the distribution of magnetic fields on the solar surface is highly inhomogeneous and that magnetic inhomogeneities outside sunspots form flux tube structures (e.g. Stenflo 1978; Zwaan 1989; Solanki 1993). Individual magnetic flux tubes are regions of intense magnetic fields that rapidly diverge in the solar chromosphere. The typical strength of the magnetic field inside these tubes at the base of the photosphere is about 1500 G but can also be less. There are turbulent motions in the solar convection zone where the tubes are rooted, but also in the solar photosphere. These motions may interact with the tubes leading to the generation of tube waves. High resolution white light observations of the Sun performed by Muller (1989), Nesis et al. (1992) and Muller et al. (1994) show that the velocity of turbulent motions can be as large as 2 km/s .

It is important to find out how efficiently the observed turbulent motions generate linear and nonlinear magnetic tube waves. The problem of generation of these waves has been treated both analytically (Musielak et al. 1989, 1995; Choudhuri et al. 1993a, b) and numerically (Huang et al. 1995; Ulmschneider & Musielak 1998). The work by Huang et al. shows that the typical wave energy fluxes carried by nonlinear transverse tube waves are of the order of $10^9 \text{ erg/cm}^2 \text{ s}$. However, the amount of energy which can be transferred to the chromosphere remains uncertain because the process of energy leakage to the external medium has not been taken into account. This is due to the use of the thin flux tube approximation by these authors. To estimate the efficiency of the leakage process, the slab structure is used to approximate a magnetic flux tube embedded in the solar photosphere (see Sect. 6.1).

Observations and numerical simulations show also evidence for the existence of large amplitude acoustic waves travelling horizontally in the upper layers of the solar convection zone (Nordlund & Dravis 1990; Cattaneo et al. 1991; Nordlund & Stein 1991; Steffen 1993; Steffen et al. 1994). It is of interest to investigate how efficiently these acoustic waves can supply energy into the magnetic flux tubes. The efficiency of this process is estimated here by using the model of two adjacent magnetic slabs (see Sect. 6.2).

6.1. Wave energy leakage

The results presented in Sect. 5 clearly show that in both cases of the longitudinal and transverse perturbation the energy carried by the body and surface waves leaks to the external medium. As a result of this process, external acoustic waves are generated. The wave energy leakage has been extensively discussed by Huang (1996) who obtained the results for magnetic slabs with $\beta < 1$ and demonstrated that more than 50% of the energy carried by transverse slab waves and almost 30% of the energy carried by longitudinal slab waves can leak out to the external medium within two wave periods. In our present work the slab structure is used to simulate a flux tube embedded in the solar photosphere and to estimate the efficiency of wave energy leakage. It is well known that the solar photosphere may be

approximated by a model consisting of two media: a magnetic region where the plasma β is of order unity or smaller, and a weak field region where β is very high. In the simulations performed here, the value of β in the slab is chosen to be 1. The external medium is assumed to be field-free, which means that β is infinite there. At the optical depth $\tau = 1$, the photospheric flux tubes have typical diameters of approximately 100 km and the sound speed is around 8 km/s. For waves with periods of around 60 seconds, the diameter of the tube is normalized to 0.21 which is taken to be equal to the slab thickness. The velocity perturbation amplitude is chosen to be 0.25, which corresponds to a velocity perturbation of 2 km/s and is in agreement with the observations (see above). Only transverse velocity perturbations are considered.

Snapshots of the resulting velocity field looks similarly as in Figs. 11 to 12. There are prominent acoustic waves in the external medium. Since the perturbations are imposed only on the slab, it is evident that a significant amount of wave energy must be leaking from the slab to the external medium. To estimate this amount of energy, we use the wave energy leakage ratio W_{leak} defined as

$$W_{leak}(t) = \frac{E_{ext}}{E_{ext} + E_{int}} \quad (19)$$

where E_{ext} and E_{int} represent the energy carried by the external acoustic waves and the internal slab waves, respectively. They are given by

$$E_{ext} = \int \epsilon dS_{ext}, \quad (20)$$

and

$$E_{int} = \int \epsilon dS_{int}, \quad (21)$$

where ϵ is the total wave energy density, and S_{ext} and S_{int} represent the part of the computational domain that is external and internal to the slab, respectively. According to Landau & Lifshitz (1959), the kinetic (ϵ_{kin}), thermal (ϵ_{therm}) and magnetic (ϵ_{magn}) energy densities contribute to the total wave energy density as

$$\epsilon = \epsilon_{kin} + \epsilon_{therm} + \epsilon_{magn}, \quad (22)$$

with

$$\epsilon_{kin} = \frac{1}{2}\rho(V_x^2 + V_y^2), \quad (23)$$

$$\epsilon_{therm} = \frac{1}{2}\gamma p \frac{\rho'^2}{\rho^2}, \quad (24)$$

and

$$\epsilon_{magn} = \frac{1}{8\pi\gamma\beta}(B_x'^2 + B_y'^2), \quad (25)$$

where V_x , V_y , ρ' , B_x' and B_y' are perturbed quantities. The time-average of $W_{leak}(t)$ defined as

$$\bar{W}_{leak} = \frac{1}{T_0} \int_0^{T_0} W_{leak} dt, \quad (26)$$

is used here as a quantitative measure of the amount of wave energy leaking to the external medium. The averaging time T_0 is chosen as 2.0 in these calculations. In general, it is desired to carry out the time average over a very long period of time. However, this is not feasible numerically as it would require an infinitely large computational domain to account for the wave spreading in time. Since the finite computational domain is used here, the simulations are stopped just before the fastest propagating wave reaches the boundary; the latter always happens when $T_0 > 2.0$.

The calculated energy leakage ratio is 0.62, which means that 62% of the energy carried by nonlinear slab waves leaks to the external medium within two wave periods. Now, applying this result to the wave energy fluxes calculated by Huang et al. (1995) for transverse tube waves, it is seen that more than half of the total wave energy flux (of 10^9 erg/cm²s) carried by these waves will be transferred to the external medium and propagate there as acoustic waves. As shown recently by Ziegler & Ulmschneider (1997a,b), the efficiency of wave energy leakage can be even higher for more realistic magnetic flux tubes.

6.2. Generation of magnetic slab waves by external acoustic waves

To calculate the efficiency of the generation of magnetic slab waves excited by external acoustic waves, the model of two identical magnetic slabs is considered (see Sect. 2) and the external medium is field-free. The slabs are placed side by side in the computational domain and the distance between them is half an acoustic wavelength (see Figs. 15 and 16). The computational domain and the grid size are similar those chosen for our longitudinal and transverse wave calculations. The slab which is located closer to the center of the computational domain is called the first slab and the other the second slab. The distance between the first slab and the center of the computational domain, where the source of the external acoustic waves is located, is one acoustic wavelength. The first slab lies at $x_1 = -1.01$, the second at $x_2 = -1.52$. The wave source is aligned along the x-direction and has a width of 1/15 of the acoustic wavelength. It must be noted that the values of these three parameters may have wide ranges in reality and that the particular values used here are chosen only for the purpose of simulation.

The numerical results obtained for $t = 2.0$ are presented in Figs. 15 and 16, which show that at the time when the simulation was stopped, the external acoustic waves have already reached both slabs. It is seen that the propagating acoustic waves pass through both slabs and, as a result, MHD body and surface waves are excited in the slabs; the latter can be even better seen in Fig. 16. Obviously, the body and surface waves generated in the first slab are stronger than those observed in the second slab. The amount of energy that is lost by the acoustic waves due to the excitation of the magnetic slab waves on the first slab is 3% and the corresponding value for the second slab is 1.1%. Although these numbers are small, it is expected that the closer the slabs are to the wave source, the more energy will be transferred to them. The amount of energy transferred must

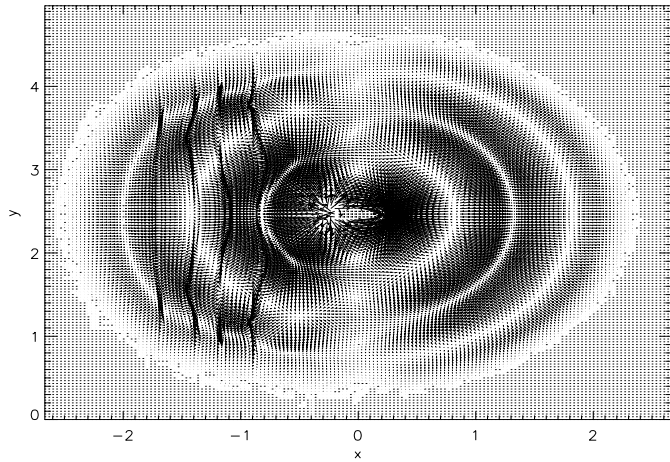


Fig. 15. The velocity field induced by the external acoustic waves generated by perturbations with $perc = 0.25$ at the center of the computational domain. Interaction of these waves with two adjacent magnetic slabs. Both slabs have $b = 0.21$ and $\beta = 1.0$. The presented results are snapshots taken at the dimensionless time $t = 2.0$.

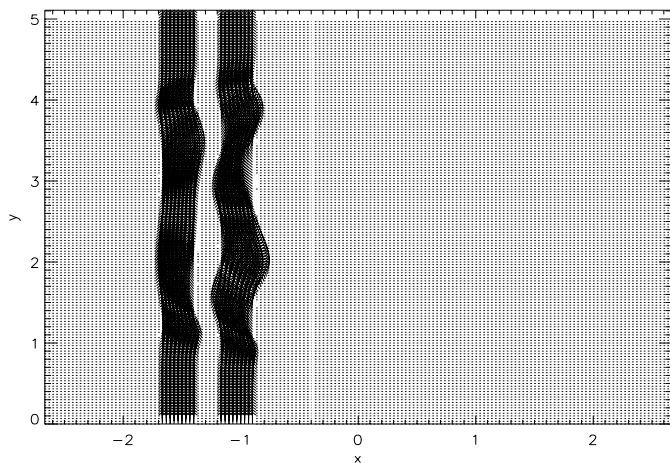


Fig. 16. The same as Fig. 14 but for the magnetic field perturbation.

also increase when the amplitude of the imposed perturbations is increased.

7. Conclusions

1. A numerical code has been developed to study the propagation of nonlinear MHD body and surface waves along magnetic interfaces and slabs. Both longitudinal and transverse MHD waves have been simulated.

2. Since an initial value problem for linear surface waves propagating along a single magnetic interface embedded in an incompressible medium has full analytical solutions, our numerical code has been tested against these solutions. A good agreement between analytical and numerical results has been found.

3. The problem of propagation of linear surface waves along a single magnetic interface embedded in a compressible medium has also been tested by comparing our results with those obtained by Wu et. al. (1996), who utilized a different numerical

scheme. Again, good agreement has been found between the results obtained by the two different numerical codes.

4. Our numerical code has been used to investigate the behavior of nonlinear MHD surface waves propagating along a magnetic slab and both longitudinal and transverse velocity perturbations with finite amplitudes were excited. The resulting wave patterns and nonlinear features have been shown and discussed.

5. The process of wave energy leakage from a magnetic slab to the field-free external medium has been studied. The obtained results show that 62% of the energy carried by transverse slab waves leaks to the external medium within two wave periods. This means that the efficiency of the energy transfer by these waves along the slab is significantly reduced.

6. The process of excitation of MHD waves in two adjacent magnetic slabs by large amplitude external acoustic waves has also been investigated. It is found that only 1 – 3% of the energy carried by these acoustic waves is transferred to the slabs, and that the efficiency of this process strongly depends on the location of the slabs relative to the source of acoustic waves and on the amplitude of these waves.

7. The leakage rates found are important for the problem of heating of magnetically structured regions in the solar and stellar atmospheres.

Acknowledgements. This work was supported by the NASA Astrophysics Theory Program under grant NAG5-3027 (P.H., Z.E.M. and P.U.), by NASA/MSFC under grant NAG8-839 (P.H. and Z.E.M.), by NSF under grant ATM-9526196 (P.H. and Z.E.M.), and by NATO under grant CRG-910058 (P.U. and Z.E.M.). Z.E.M. also acknowledges the support of this work by the Alexander von Humboldt Foundation.

References

- Bertin G., Coppi B., 1985, ApJ 298, 387
- Brackbill J.U., Barnes D.C., 1980, J. Comp. Phys. 35, 426
- Cattaneo F., Brummell N.H., Toomre J., Malagoli A., Hulbert, N.E., 1991, ApJ 370, 282
- Chen L., Hasegawa A., 1974, Phys. Fluids 17, 1399
- Choudhuri A.R., Auffret H., Priest E.R., 1993a, Sol. Phys. 143, 49
- Choudhuri A.R., Dikpati M., Banerjee D., 1993b, ApJ 413, 811
- Evans C.R., Hawley J.F., 1988, ApJ 332, 659
- Forbes T.G., Priest, E.R., 1987, Rev. Geophys. 25, 1583
- Goedbloed J.P., Halberstadt G., 1994, A&A 286, 265
- Goossens M., 1994, Space Sci. Rev. 68, 51
- Herbold G., Ulmschneider P., Spruit H.C., Rosner R., 1985, A&A 145, 157
- Hirsch C., 1990, Numerical Computation of Internal and External Flows. John Wiley & Sons, New York
- Huang P., 1995, Ph.D. Thesis, Univ. of Alabama, Huntsville
- Huang P., 1996, Phys. Plasmas 3, 2579
- Huang P., Musielak Z.E., Ulmschneider P., 1995, A&A 279, 579
- Landau L.D., Lifshitz E.M., 1959, Fluid Mechanics. Pergamon Press, London
- Lanzerotti L.J., Southwood D.J., 1979, In: Kennel C.F., Lanzerotti L.J., Parker E.N. (eds.) Solar System Plasma Physics. North-Holland, New York, p. 109
- Lanzerotti L.J., Fukunishi H., Hasegawa A., Chen L., 1973, Phys. Rev. Lett. 31, 624

- Lee M.A., Roberts B., 1986, *ApJ* 301, 430
- Marder B., 1987, *J. Comp. Phys.* 68, 48
- Muller R., 1989, In: Rutten R.J., Severino G. (eds.) *Solar and Stellar Granulation*. Kluwer Academic Publ., Dordrecht, p. 101
- Muller R., Roudier Th., Vigneanu J., Auffret H., 1994, *A&A* 283, 232
- Musielak Z.E., Suess S.T., 1988, *ApJ* 330, 451
- Musielak Z.E., Rosner R., Ulmschneider P., 1989, *ApJ* 337, 470
- Musielak Z.E., Rosner R., Gail H.P., Ulmschneider P., 1995, *ApJ* 448, 865
- Narain U., Ulmschneider P., 1996, *Space Sci. Rev.* 75, 453
- Nesis A., Bogdan T.J., Cattaneo F., et al., 1992, *ApJ* 399, L99
- Nordlund A., Dravins D., 1990, *A&A* 238, 155
- Nordlund A., Stein R.F., 1991, In: Crivellari L., Hubeny I. (eds.) *Stellar Atmospheres: Beyond Classical Models*. NATO ASI Series, Kluwer Academic Publ., Dordrecht, p. 263
- Orlanski I., 1976, *J. Comp. Phys.* 21, 251
- Poedts S., Goedbloed J.P., 1997, *A&A* 321, 935
- Poedts S., Tóth G., Beliën A.J.C., Goedbloed J.P., 1997, *Sol. Phys.* 172, 45
- Roberts B., 1981a, *Sol. Phys.* 69, 27
- Roberts B., 1981b, *Sol. Phys.* 69, 39
- Roberts B., 1991, In: Priest E.R., Hood A.W. (eds.) *Advances in Solar Solar System Magnetohydrodynamics*. Cambridge Univ. Press, Cambridge, p. 105
- Roberts B., Webb A.R., 1978, *Sol. Phys.* 56, 5
- Solanki S.K., 1993, *Space Sci. Rev.* 63, 1
- Spruit H.C., 1981, *A&A* 98, 155
- Spruit H.C., Roberts B., 1983, *Nat* 304, 401
- Steffen M., 1993, *Habil. Thesis*, Univ. Kiel, Germany
- Steffen M., Freytag B., Holweger H., 1994, In: Schüssler M., Schmidt W. (eds.) *Solar Magnetic Fields*. Cambridge Univ. Press, Cambridge, p. 298
- Stenflo J.O., 1978, *Rep. Prog. Phys.* 41, 865
- Ulmschneider P., Musielak Z.E., 1998, *A&A*, in press
- Ulmschneider P., Zähringer K., Musielak Z.E., 1991, *A&A* 241, 625
- Takahashi K., McPherron R.L., 1984, *Space Sci. Rev.* 35, 301
- Wentzel D.G., 1979, *ApJ* 227, 319
- Wu S.T., Xiao Y.C., Musielak Z.E., Suess S.T., 1996, *Sol. Phys.* 163, 291
- Ziegler U., Ulmschneider P., 1997a, *A&A* 324, 417
- Ziegler U., Ulmschneider P., 1997b, *A&A* 327, 854
- Zwaan C., 1989, In: Von der Lühe O. (ed.) *High Spatial Resolution Solar Observations*. National Solar Obs. Sunspot, NM, p. 420